sustainability

MDPI

Article

Precision Ventilation in an Open-Plan Office: A New Application of Active Chilled Beam (ACB) with a JetCone Feature

Haider Latif [1], Samira Rahnama [1], Alessandro Maccarini [1], Goran Hultmark [2], Peter V. Nielsen [1] and Alireza Afshari [1,*]

[1] The Department of the Built Environment, Aalborg University, 2450 Copenhagen, Denmark; hala@build.aau.dk (H.L.); sar@build.aau.dk (S.R.); amac@build.aau.dk (A.M.); pvn@civil.aau.dk (P.V.N.)
[2] Indoor Climate Solutions, Lindab A/S, 3520 Haderslev, Denmark; goran.hultmark@lindab.com
* Correspondence: aaf@build.aau.dk

Abstract: Mixing ventilation systems effectively improves thermal comfort in open-spaces due to adequate turbulent mixing of the cold stream with ambient air. This study introduces the concept of precision ventilation for achieving local thermal comfort in a mixing ventilation system. This precision ventilation system provides asymmetrical airflows from an active chilled beam (ACB) to each of the office occupants. These ACBs provide air velocities with different magnitudes and directions. To achieve different magnitudes and directions, JetCones are used to vary the airflow in different parts of the ACB. The performance of the precision ventilation system was analyzed using full-scale laboratory experiments and computational fluid dynamic (CFD) simulations. The full-scale laboratory experiments were conducted in a 4.2 m × 3 m × 2.8 m (L × W × H) thermal isolated room with an open-plan dual desk-chair setup. The jet-cones in the ACB unit were adjusted to throw the required amount of flow to the occupants. The occupants had different metabolic rates of 1.2, 1.4, and 1.6 in a warm office space. The room set point temperatures varied between 23 and 26 °C. The experimental and CFD results show that occupants facing symmetrical airflow distribution and with a constant 1.2 metabolic rate had a similar PMV index. The occupants with 1.2, 1.4, and 1.6 metabolic rate were exposed to asymmetrical airflows, i.e., 30%, 58%, and 70% of the total airflow. Occupants with higher metabolic rates were kept thermally neutral, in the −0.5 to +0.5 PMV range, by increasing the air velocity and room temperature to 0.4 m/s and 25 °C, respectively.

Keywords: active chilled beams; asymmetrical airflows; JetCones; metabolic rates; precision ventilation

Citation: Latif, H.; Rahnama, S.; Maccarini, A.; Hultmark, G.; Nielsen, P.V.; Afshari, A. Precision Ventilation in an Open-Plan Office: A New Application of Active Chilled Beam (ACB) with a JetCone Feature. *Sustainability* **2022**, *14*, 4242. https://doi.org/10.3390/su14074242

Academic Editor: Giouli Mihalakakou

Received: 5 March 2022
Accepted: 31 March 2022
Published: 2 April 2022

1. Introduction

The increasing demand for HVAC in buildings has led researchers towards technological advancements in order to provide desirable thermal comfort for building occupants. Currently, people spend 80–90% of their time indoors with an increasing reliance on air conditioning and mechanical ventilation (ACMV) systems to have a comfortable indoor environment [1]. Similarly, people spend on average 40 h per week in their offices [2]. This dependency has led many researchers to bring greater advancements to existing ACMV systems, which can provide desirable indoor climate solutions for office buildings.

Mixing ventilation [3] is one of the most used ventilation systems for providing space cooling. It involves moving cold air from ceiling level to the floor, driven by momentum and density difference. The falling jets are mixed with ambient air and this establishes a uniform temperature level with low temperature stratification. Active chilled beams (ACBs) are a typical example of mixing ventilation systems that are fixed in the ceiling to make use of the Coandă effect to distribute room air. According to the definition, a Coandă effect is the tendency to entrain fluid from the surroundings so that a region of lower static pressure develops to have the free jet attached to the ceiling [4,5]. This effect is one of the

prominent feature of the ACBs. Rhee et al. concluded that ACBs are considered successful in providing acceptable thermal uniformity compared to other conventional air distribution systems, e.g., displacement ventilation [6].

Thermal comfort is defined as the state of mind that expresses satisfaction with the thermal environment [7]. The literature shows that thermal comfort preferences may vary among office occupants due to a change in metabolic rate, gender, age, and health [8]. Therefore, building occupants might perceive thermal comfort differently, even when they are exposed to the same thermal environment [9]. Individual thermal comfort is an issue that needs to be addressed, which involves personalized control of the micro-climate around the individual according to their needs. Figure 1 shows six factors that affect the thermal comfort of any individual [10].

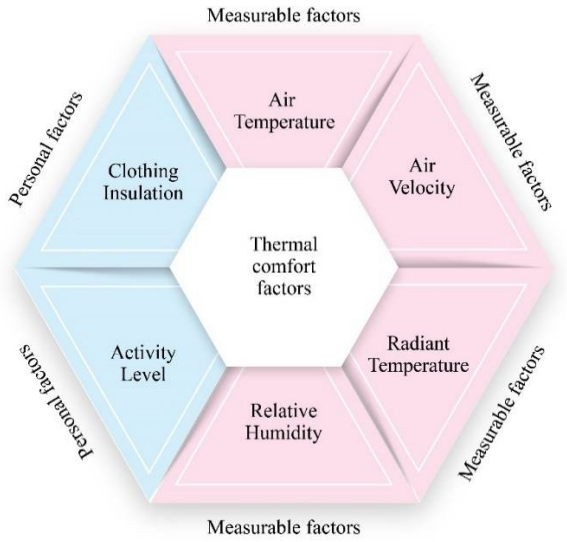

Figure 1. Thermal Comfort Parameters.

The human body has a constant internal temperature and the thermoregulatory system of the body tries to maintain this, despite a wide range of environmental factors [11]. Any imbalance due to inappropriate thermal conditions may adversely affect work productivity in a working environment [12,13]. In addition, the inability to provide individual thermal comfort is considered one of the drawbacks of conventional ACMV systems [14]. An alternative to mixing ventilation system, the personalized ventilation (PV) systems (also known as task ambient systems) [15], have been studied for the past two decades to meet individual thermal comfort requirements in offices. These systems make use of multiple air terminal devices (ATDs) on office workstations to build micro-climate zones. Despite its advantages, PV applications are limited in the HVAC market due to use of multiple ATDs, which appropriately does not fit building aesthetics. Secondly, direct airflow from ATDs to the human body may cause risk of draft or irritation [16]. PV systems coupled with mixing ventilation systems have been studied in order to improve individual thermal comfort [17], but efficiency of these hybrid systems is dependent on the location of multiple ATDs (used in PV systems) to promote mixing [18].

By directing airflow from an ACB outlet that moves along the ceiling towards different zones of a single space, this study presents a mixing ventilation system in a different way. In the past, ACBs used to maintain uniformity of air distribution in rooms have been studied [19,20], but these systems have not been used for individual thermal comfort applications. The aim of this study is to present efficient air mixing with optimal air speeds around occupants to fulfill individual thermal comfort requirements, according to different metabolic rates of the occupants. To enable targeted cooling by varying the air velocity's magnitude and direction through adjustment pins, see Figure 2. This precision ventilation system uses ACB units with a JetCone feature [21].

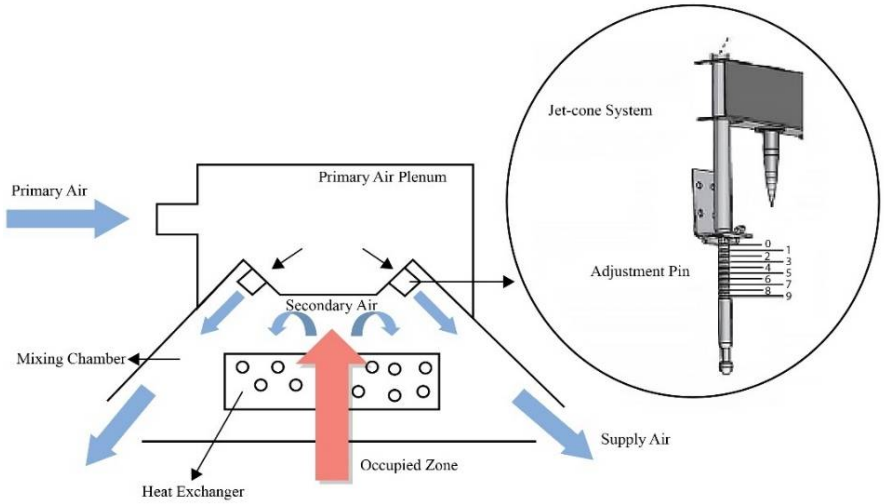

Figure 2. ACB Unit with JetCone system.

Zhang et al. suggested that the room temperatures are often raised for indoor climate studies to save energy [22]. The thermal comfort for these elevated room temperatures can be maintained by increasing the room air velocities. Therefore, this experimental simulation study is conducted for a warm office environment by creating high and low velocity zones around occupants to achieve individual thermal comfort.

2. Experimental Setup

2.1. ACB with JetCones

In the study, the ACB unit with angled nozzles was used, as shown in Figure 3. The plexus was tested and rated according to Danish Standards Foundation DS/EN 15116 [23]. The JetCone feature in the plexus provided control over the primary airflow in the nozzles and pressure in the air inlet. In addition, the nozzles are directed to create a 360° airflow pattern. Four adjustment regulators at each corner gives the ability to adjust the airflow from the ACB to the different parts of the room. These adjustment regulators provide 10 different positions each, which gives 40 different settings to control air diffusion, supply air volume, and pressure.

Figure 3. Schematic drawing of an ACB unit with JetCones [24].

The asymmetrical airflow patterns were achieved by adjusting regulator pins from positions 0 to 9. Position 0 of the adjustment regulator allowed minimum airflow coming out of the ACB outlet, whereas pin position 9 allowed maximum airflow to pass through the specific side of the beam outlet. Table 1 shows the complete features of the plexus used in this study.

Table 1. ACB-system details.

Units	Values
ACB Dimensions (L × W × H)	0.6 m × 0.6 m × 0.2 m
ACB Unit	1
Functions	Cooling, Heating & Ventilation
Operating System	Cooling 2-pipe system
Distribution profile	Radial
Capacity	769 W
Primary airflow rate	20 L/s (fixed)
Supply Air temperature	21 °C

The plexus has a standard Ø12 mm water pipe and Ø125 mm horizontal air duct which can be used for cooling, heating, and ventilation applications. This study was limited only to individual comfort through cooling.

2.2. ACB Airflow Distribution

The discharge velocities at 16 different positions of the ACB unit openings were measured to analyze the initial data and airflow distribution. The airflow on each side of the plexus opening was different due to radial discharge and different JetCone settings. The 16 equally spaced velocities at the beam outlet were measured to observe the airflow patterns with three different JetCone settings. Initially, three JetCone settings were measured under non-isothermal conditions (see Figure 4). These include:

1- All four-pins at position 5 to have uniform air distribution.
2- Two-pins at position 5 and two at position 0 to have more primary flow pushed towards one half of the plexus.
3- Two-pins at position 9 and two at position 0 to have maximum discharge on one side and minimal discharge from the remaining beam half.

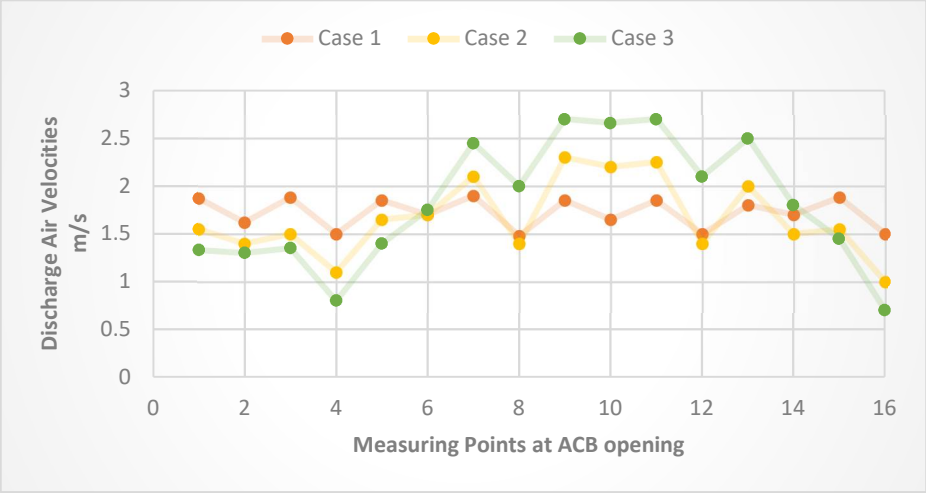

Figure 4. Discharge Velocities measured at ACB opening with different ACB pin-settings.

Figure 4 shows that the discharge velocities in case 1 are uniform due to the same pin settings, whereas case 2 and case 3 have maximum discharge velocities in-between points 6 and 14, as this is where JetCones are partially or fully opened. Figure 5 shows the airflow distribution of all three cases. In case 1, the discharge velocities show symmetrical airflow distribution from the JetCones. This means 50% of the total airflow is discharged from each half of the plexus. In case 2, the discharge velocities measured had 58% and 42% of airflow division for the pin positions at 5 and 0. In case 3, the airflow from the sides of the beam outlet with pin position 9 had greater airflow than the sides on position 0. The magnitude of velocities for the third case shows that JetCones opened at position 9 discharge (maximum)

70% of the airflow, while the ones with the pin position at 0 only allow 30% of the airflow from the beam outlet. However, the amount of primary airflow is kept constant.

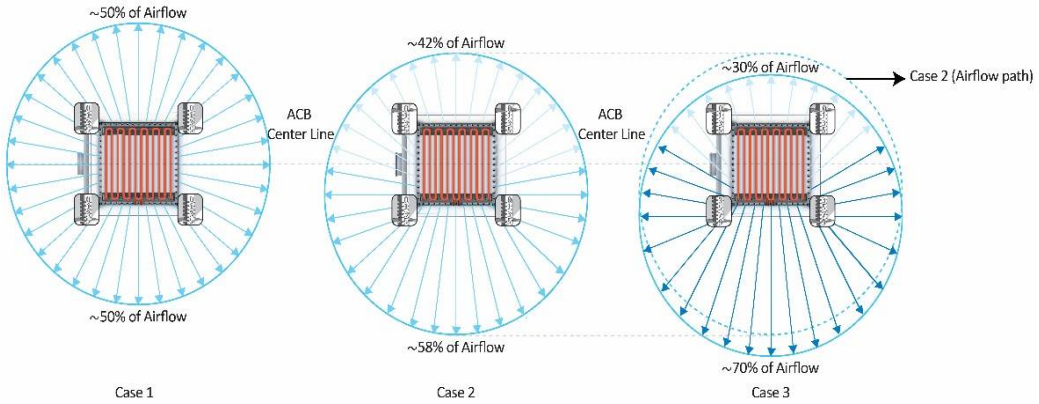

Figure 5. Airflow distribution (Cases 1, 2, and 3).

Table 2 shows the flow division, at a constant primary airflow rate of 20 l/s, based on nozzle pressures set according to the pin positions. The full-scale experimental study for targeted air distribution is applied for the three cases. The measured discharge air velocities were used as inlet velocities for CFD boundary conditions.

Table 2. Pin position properties.

Cases	Adjustment Pin Settings	Static Nozzle Pressure Loss Δp_{stat} (Pa) (Manufacturer's Data)	Airflow Division (Measured) (%)
Case 1	5 + 5 + 5 + 5	75	50/50
Case 2	0 + 0 + 5 + 5	300 (Estimated)	58/42
Case 3	0 + 0 + 9 + 9	80	70/30

2.3. Test Room

The full-scale laboratory experiments were conducted in a room with dimensions 4.2 m × 3 m × 2.8 m (L × W × H) at Aalborg University Copenhagen. The experiments were carried out with cooling power of ACB balanced with heat sources in the room. The room walls, ceiling, and floor were kept adiabatic without the influence of any solar sources. The open-plan office layout of the test room with two workstations was chosen due to its common use for conducting experiments on ACBs [25]. The ACB was installed in the middle of the ceiling, i.e., 1.8 m away from the two sides (north and south direction), as shown in Figure 6. Table 3 shows the test room parameters set during the experiments.

Table 3. Test room details.

Parameters	Values
Office area	12 m^2
Occupant density	6.0 m^2/person (2 persons)
Office Equipment	2 workstations (2 dummies, Two computers, lights)
Set Room Temperatures	23–26 °C
Occupants (Sensible heat)	65 W/m^2, 80 W/m^2 and 95 W/m^2 per dummy
Total Average Zone Load	510 Watts

The position of the two dummies (each 1.4 m tall) were 1.85 m apart so that their thermal flux had a negligible effect on each other. These dummies are separated by open-plan 40 cm × 75 cm desks (L × W) under the plexus as shown in Figure 6. The human heat source was replicated by placing electric bulbs inside the dummies. The metabolic

rate of each dummy was varied by changing the number and capacity of the electric bulbs installed inside. Other heat sources were computers and lamps (see Appendix A).

Figure 6. Office setup.

The air velocity measurements in the test room were carried out by locating sensors along the length of the room. For all three cases, the measuring points were set in the occupied space to observe airflow distribution inside the room. The air temperature and velocity distributions were measured on points such that heat flux from the dummy did not affect the measurements. The measurements were taken during summer (May–October). The room temperature varied between 23 °C and 26 °C. The measurements were taken at 20 different points at 0.1 and 1.1 m above the floor located at two different zones (see Figure 7). Zone 2 towards the north wall was exposed to high air velocities for cases 2 and 3. The measuring points in both zones were equally distributed such that the airflow distribution in each case could be evaluated.

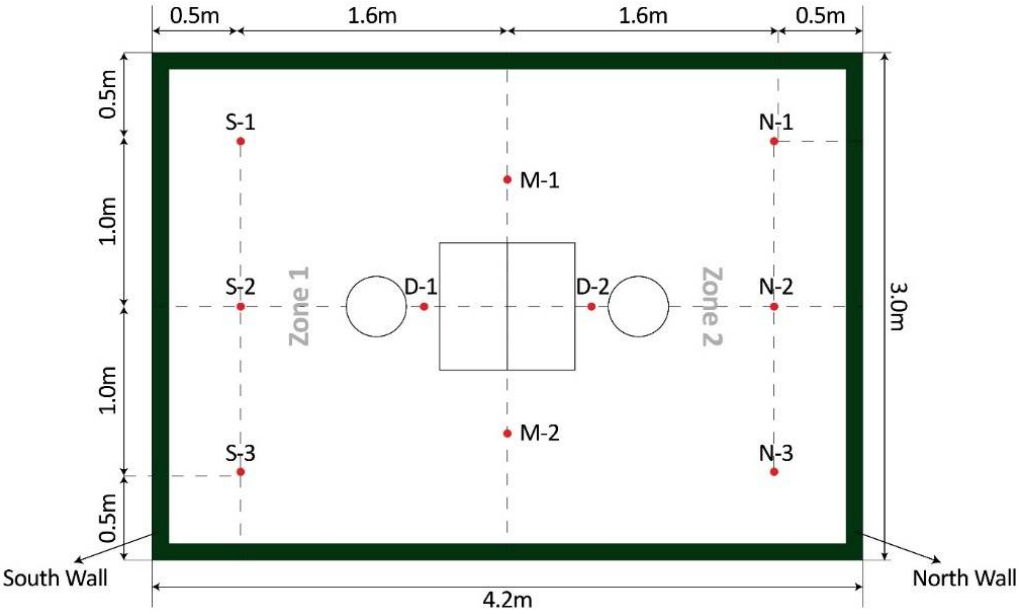

Figure 7. Plan view of test room with the measuring points.

N and S points in Figure 7 were 0.5 m from the north and south walls, respectively. M1 and M2 points in the middle of the room were taken to trace the velocity magnitude. The velocity and temperature data at D1 and D2 points (located in zone 1 and 2, respectively) were used for thermal comfort measurements of the human dummy at different metabolic rates.

2.4. Thermal Comfort Criteria

In the current study, predicted mean vote (PMV) and predicted percentage dissatisfied (PPD) indices are used for evaluation of thermal comfort in an enclosed environment [26]. The expressions of Fanger's PMV and PPD models are given by the Equations (1) and (2).

$$\begin{aligned} PMV = (0.303e^{-0.036M} + 0.028)\,\{(M - W) - 3.05 \times 10^{-3}\,[5733 - 6.99(M - W) - p_a] - \\ 0.42\,[(M - W) - 58.15] - 1.7 \times 10^{-5}\,M\,(5867 - p_a) - 0.0014\,M\,(34 - T_a) - 3.96 \times \\ 10^{-8}\,f_{cl}\,[(T_{cl} + 273)^4 - (T_r + 273)^4] - f_{cl.}h_c(T_{cl} - T_a)\}, \end{aligned} \quad (1)$$

$$PPD = 100 - 95\exp\,[-\,(0.03353PMV^4 + 0.2179PMV^2)] \quad (2)$$

PMV was calculated based on mean values of the local air temperature (T_a), mean radiant temperature (T_r), and local air velocity (V_r). As it is generally very close to air temperature in most cases, the mean radiant temperature was assumed equal to air temperature [27]. Equation (1) shows M as the metabolic rate which varies according to activity level, whereas the effective mechanical power (W) is assumed zero. The clothing surface area (f_{cl}) and the convective heat transfer coefficient (h_c) were calculated iteratively. The clothing value is given as 0.6 clo (for summers) due to changing clothing habits of office occupants' w.r.t seasons [28]. The activity level in offices may differ between individuals. Some stay simply seated (relaxed) to getting involved in sedentary or light office activities. The metabolic rates were assumed to be 1.2 met (65 W m^{-2}) to 1.6 (95 W m^{-2}) met per occupant to have different activity levels (heat release) [29]. The heat balance was established by creating high air velocities zones at high room temperatures to maintain individual thermal comfort for occupants with increased metabolic rates. In the present study, draught rate (DR) is not considered due to the need for higher air velocities for the occupants with high metabolic rates at room air temperatures up to 26 °C. High air velocities are created around the dummies to maintain body heat balance (with respect to the activity level) and PMV values within the acceptable thermal comfort range. Vertical velocity and temperature measurements near the human dummy were measured by two moveable poles attached with Dantec hot sphere anemometers at steady conditions (see Figure 8). The testing area for PMV measurements is set at the vicinity of the dummy as a vertical line in zones one and two. These parameters were measured at three heights equal to head level (1.1 m), abdomen (0.6 m), and ankle (0.1 m) from the floor of a seated person [30]. The dummies (located in two different zones) with variable metabolic rates exposed to different air velocities (ranging from 0.1 m/s to 0.4 m/s) were used for PMV-PPD measurements. The acceptable thermal comfort range between $-0.5 < PMV < 0.5$ was considered appropriate [26]. The room air velocity was measured using Dantec hot sphere anemometers with an absolute accuracy of ±2% of the reading (between the range of 0 and 1 m/s) [31]. During the measurements, the average velocity data were collected with a sample time of 180 s according to the requirement for the measurement of the indoor air velocity in EN 13182:2002 [32].

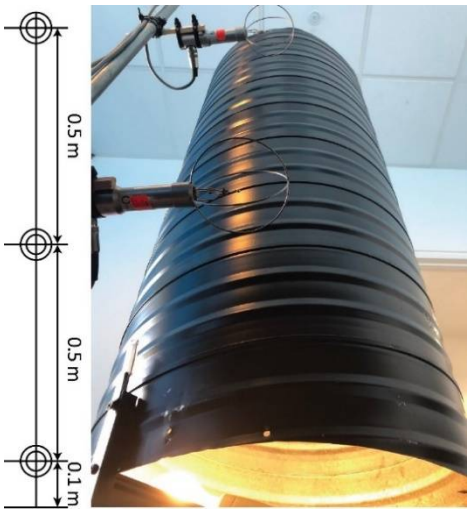

Figure 8. Vertical measuring points with hot sphere anemometers along the dummy.

3. Simulation Model

The geometry of the ACB unit was made circular and simplified to reproduce radial distribution pattern (see Figure 9a). The inlet faces were filleted with 0.03 m radius to have discharge flow parallel to the ceiling surface. The total area of the inlet opening was 0.04 m^2. The opening of the ACB was divided into 16 equal divisions to have variable velocity spread along the ceiling with respect to JetCone settings. The airflow from each quarter of the round ACB outlet was controlled by one adjustment pin (Figure 9b). The geometry of the ACB was reduced to only the bottom part for simplicity and the magnitude of airflow and temperature of the inlet surfaces were set as a resultant of both primary and secondary airflows.

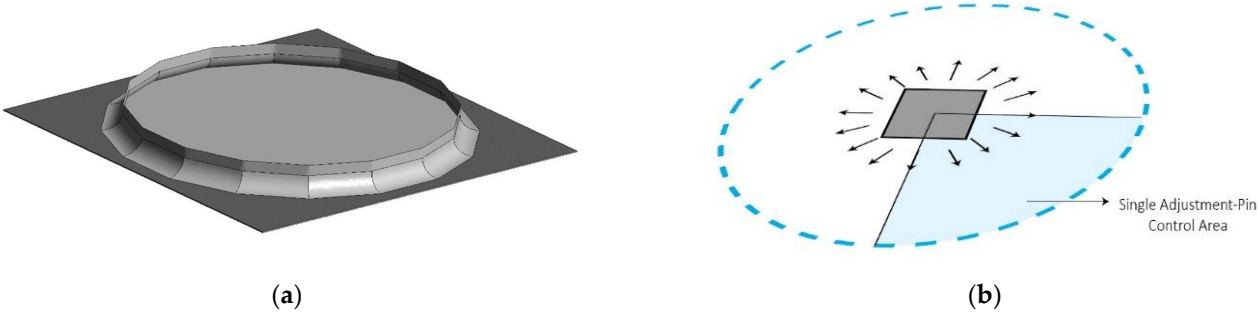

(**a**) (**b**)

Figure 9. (**a**) ACB terminal unit geometry (**b**) Radial flow distribution with pin controls.

The geometry of the room with the actual dimensions was made on the SolidWorks software. The geometry consisted of two fully equipped workstations positioned centrally, along with a radial geometric ACB unit fitted at ceiling level, as shown in Figure 10. The outlet was positioned on one of the walls, next to the workstation towards the north side. The heat loads used in the measurements comprised computers with a human dummy (Appendix A). The cylindrical dummy was applied with the thermal heat flux according to different metabolic rates.

The SolidWorks geometric model was imported to ANSYS FLUENT 17.1 version for the CFD simulations. Tetrahedral meshes were generated in the entire computational domain with fine local meshing done near the critical areas such as ACB supply inlets and all heat sources (Appendix A). The pressure-based solver was used for the simulations under steady state conditions. The RNG k-ε turbulence model was selected for the simulations due to better accuracy than other RANS models for indoor airflow simulations [33–35] and less computational cost than LES models [36,37]. Boundary conditions for the velocity inlets of all three cases were used based on the experimental data collected from preliminary

ACB measurements (see Figure 4). The total inlet flow coming out of the inlet opening was 60 L/s (sum of primary and secondary airflows), distributed according to the pin positions (see Figure 5). The convective heat fluxes (see Table 3) were applied to describe the boundary condition of the human body according to metabolic rates of three cases. Other heat sources were also given thermal heat fluxes (Appendix A). The SIMPLE numerical algorithm was selected for coupling pressure and momentum equations and the criteria for convergence was set 10^{-6} [38].

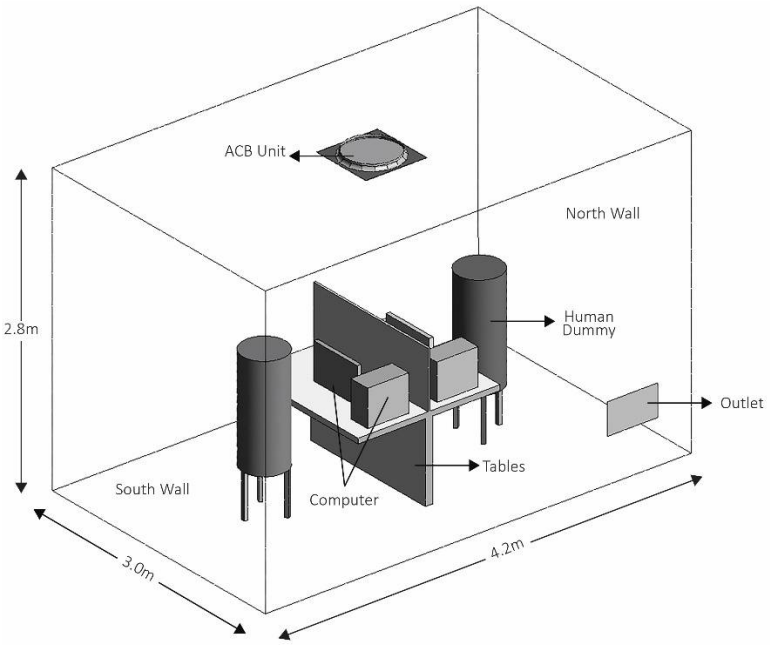

Figure 10. Test room model.

4. Results and Discussion

4.1. Velocity Distribution

Velocity measurements were taken after attaining the steady state conditions inside the room. Measurements were taken at the locations shown in Figure 7 and two different heights (0.1 m and 1.1 m above the floor) to observe velocity distribution. Table 4 shows the average and maximum air velocities for all three cases.

Table 4. Maximum/Average Air Velocity distribution measured in the room.

Maximum/Average Air Velocity	Case 1	Case 2		Case 3	
	Average Velocity	Low Velocity End	High Velocity End	Low Velocity End	High Velocity End
0.1 m	0.14	0.15/0.12	0.28/0.23	0.11/0.08	0.4/0.35
1.1 m	0.18	0.14/0.11	0.25/0.21	0.1/0.09	0.34/0.32

There were no high and low velocity zones for case 1, so only average room air velocities were considered at the measuring points. Case 2 and 3 shows considerable high air velocities towards the north wall of the room due to greater directed airflow. Velocities at 1.1 m above the floor region were found to be slightly higher than at the 0.1 m region. Maximum velocities up to 0.3 and 0.4 m/s were achieved in cases 2 and 3, respectively, whereas uniformity in air distribution was observed in case 1, with an average velocity of 0.16 m/s across the room.

Horizontal velocity profiles in Figures 11–13 show that the velocities from the north and south walls were found to decrease towards the middle of the room. The air velocities at the middle of the room, at points M1 and M2 were seen <0.1 m/s due to minimal directed

flow towards these points. CFD showed similar results of the experiments with a variation of +10% (Appendix A). Figure 14 shows vertical air velocity and temperature points (D1 and D2) for the three cases in the occupied zone.

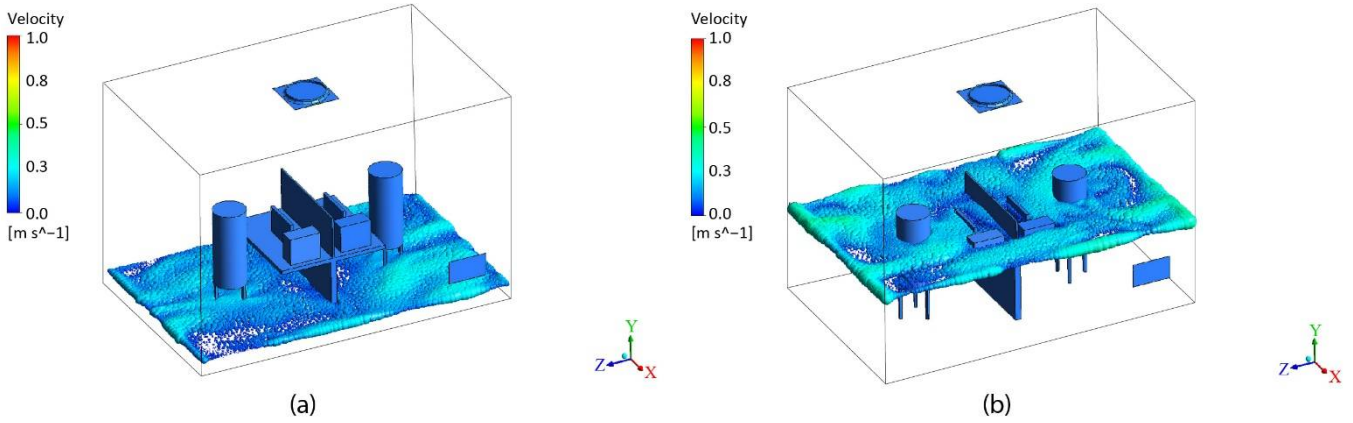

Figure 11. Case 1 Air Velocity Distribution (**a**) 0.1 m from the floor (**b**) 1.1 m from the floor.

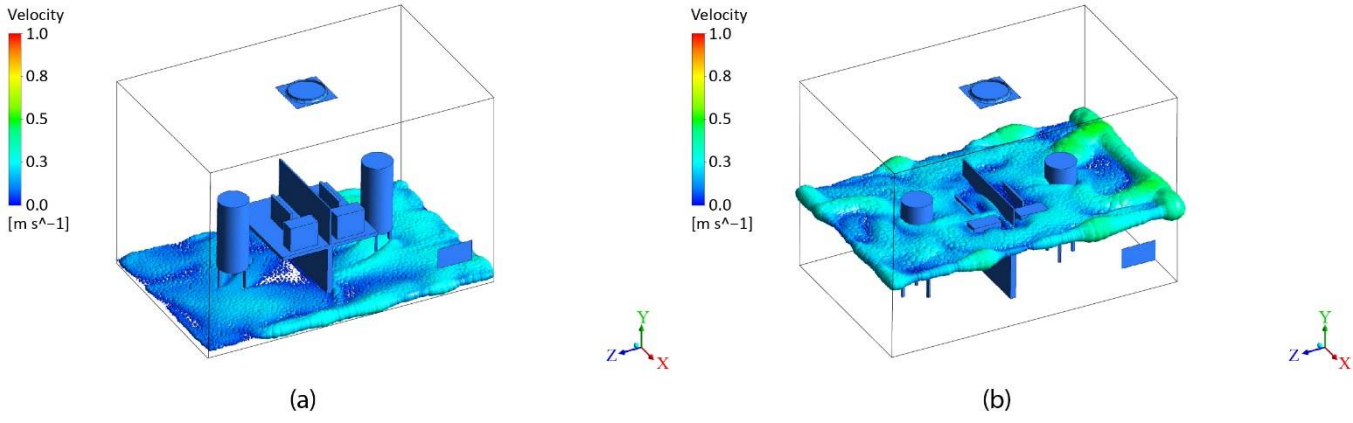

Figure 12. Case 2 Air Velocity Distribution (**a**) 0.1 m from the floor (**b**) 1.1 m from the floor.

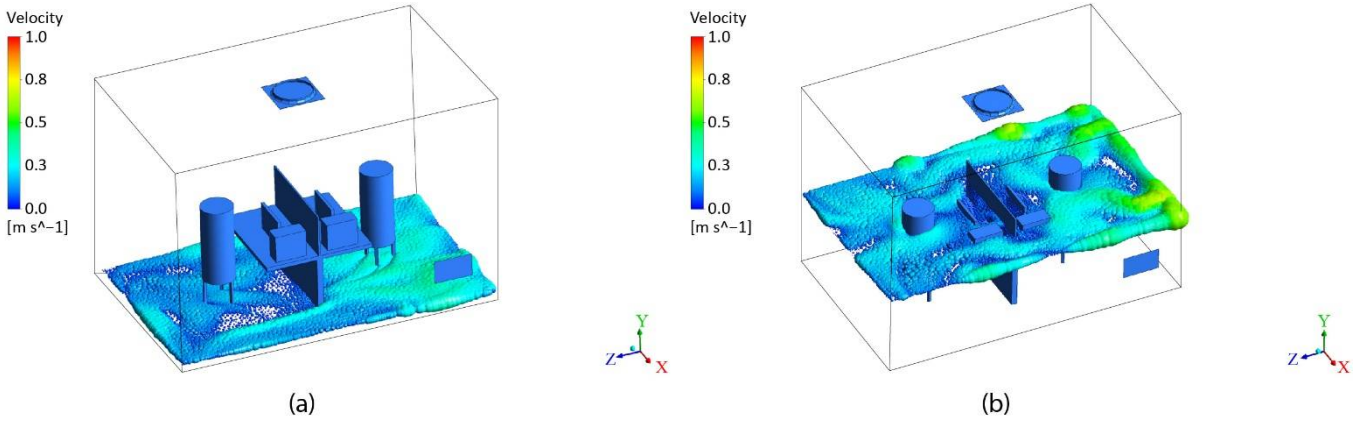

Figure 13. Case 3 Air Velocity Distribution (**a**) 0.1 m from the floor (**b**) 1.1 m from the floor.

During the measurements, the local air velocities near the head were found slightly higher than the ankle region. Figure 14 shows that the vertical temperature difference in the occupied zone between the height of the ankle and head was found maximum up to 1 °C. This temperature difference (less than 3 °C) is considered acceptable according to the ISO 7730 standard [26]. The horizontal temperature difference (for all the cases)

between high and low velocity zones was also found within ±1 °C range. However, the air temperature stratification was 0.5 °C in the center of the test room from the height of 1.0 to 2.8 m from the floor. The rise of temperature in the room was not seen to influence the velocity distribution around occupants.

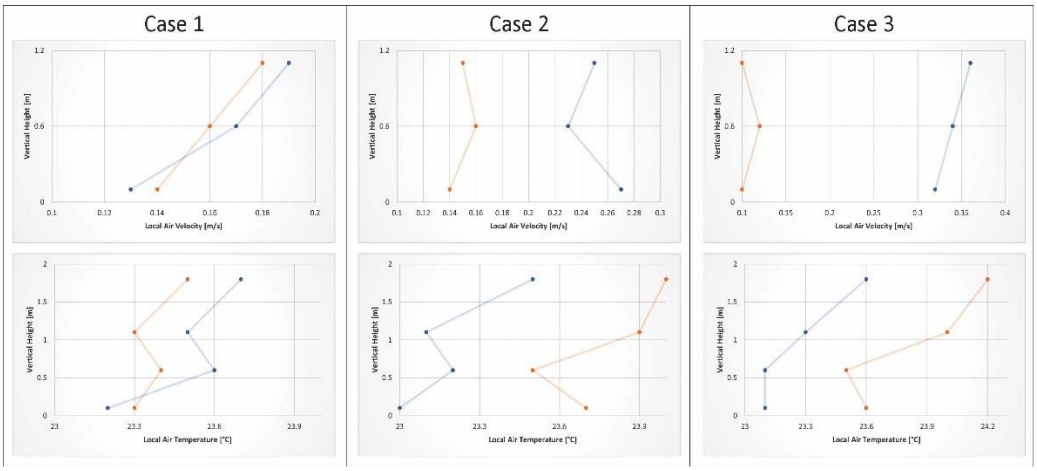

Figure 14. Vertical Local Air Velocity and Temperature distribution in the Occupied Zone.

4.2. Thermal Comfort Calculations

Thermal comfort calculations are made based on measurements in the room. The increase in local air velocity near thermal dummies results in higher convective heat transfer [39]. This change in this environmental variable is required to preserve the heat balance between human body and the surrounding environment. The metabolic rates are kept at these combinations, 1.2 met, 1.4 met, and 1.6 met for the three cases at constant Relative Humidity (RH). Case 1 included both the dummies with 1.2 metabolic rates. The metabolic rates for only dummy 2 (zone 2) in cases 2 and 3 were increased to 1.4 and 1.6, respectively. The thermal comfort for each occupant is evaluated in the mock-up office room using PMV and PPD indices (see Tables 5–7). The PMV and PPD values of two persons with a height of a seated person are determined by taking mean values of air temperature, radiant temperature, and air velocity at locations D1 and D2 (in zones 1 and 2) (see Figure 7). The mean values were taken at heights 0.1 m, 0.6 m, and 1.1 m.

Table 5. Case 1 Measured temperature, RH and Local Air velocities, and calculated PMV & PPD.

Input Data (Dummy 1 and Dummy 2)			PMV		PPD (%)
Ta = Tr (°C)	**RH (%)**	**Vr (m/s)**	**Dummy 1 (met. 1.2) in Zone 1**	**Dummy 2 (met. 1.2) in Zone 2**	
23	60	0.14	**−0.61**		12.7
24			−0.29		6.7
25			0.04		5
26			0.36		7.7

Table 6. Case 2 Measured temperature, RH and Local Air velocities, and calculated PMV & PPD.

Ta = Tr (°C)	Dummy 1: Input Data		PMV	PPD (%)	Dummy 2: Input Data		PMV	PPD (%)
	RH (%)	**Vr (m/s)**	**Dummy 1 at Low Velocity Zone (met. 1.2)**		**RH (%)**	**Vr (m/s)**	**Dummy 2 at High Velocity Zone (met. 1.4)**	
23	60	0.12	−0.54	11.2	60	0.25	−0.23	6.1
24			−0.23	6.1			0.05	5
25			0.09	5.2			0.32	7.1
26			0.41	8.4			0.6	12.5

Table 7. Case 3 Measured temperature, RH and Local Air velocities, and calculated PMV & PPD.

Ta = Tr (°C)	Dummy 1: Input Data		PMV	PPD (%)	Dummy 2: Input Data		PMV	PPD (%)
	RH (%)	Vr (m/s)	Dummy 1 at Low Velocity Zone (met. 1.2)		RH (%)	Vr (m/s)	Dummy 2 at High Velocity Zone (met. 1.6)	
23	60	0.10	−0.47	9.7	60	0.38	−0.01	5.0
24			−0.17	5.6			0.26	6.4
25			0.14	5.4			0.51	10.5
26			0.46	9.4			**0.77**	17.4

Table 5 shows PMV and PPD for case one where there is uniform distribution of airflow from the ACB with all JetCones at position 5. In order to comply with ASHRAE 55, the recommended thermal limit on PMV scale is between −0.5 and 0.5 [26]. The range of PMV for both Dummy 1 and Dummy 2 range from −0.61 to 0.36 with set point temperatures from 23–26 °C. The metabolic rate was also kept constant, i.e., 1.2 for both the occupants, representing same activity and health condition. The occupants feel slightly cool at 23 °C and almost thermally neutral and satisfied at 24–26 °C.

Table 6 shows PMV and PPD for case 2 where there is medium level flow (see Figure 5) directed towards Dummy 2 with met. 1.4 (high heat release) in the zone 2. On the other side, Dummy 1 with met. 1.2 in zone 1 is influenced by the remaining 42% of the flow. Results shows acceptable individual thermal comfort is reached for both the occupants due to targeted velocity distribution. Dummy 1 and Dummy 2 have PMV ranges −0.54 to 0.41 and −0.23 to 0.6, respectively. Hence, the occupant with elevated metabolic rate gets the high air velocity to maintain the feeling of neutral sensation.

Table 7 shows PMV and PPD for normal and increased metabolic rate of occupants to validate the applications of ACB for individual thermal comfort. Results indicate occupants with 1.6 met maintained thermal sensation within the comfortable range of −0.5 and +0.5 [26,40]. However, Dummy 2 with a metabolic rate of 1.6 had PMV index exceeding +0.5 at air temperature of 26 °C. Hence, thermal comfort level was reached to a maximum temperature range of 25 °C with elevated air velocities. Further increases in air temperature leads to the feeling of being slightly warm for the occupant.

The variable supply velocities from a single ATD, i.e., ACB directed towards each dummy, resulted in variations in local air velocity around dummies, with percentage of dissatisfied (PPD) less than 15%, even with increased metabolic rates. Figure 15 shows that suitable velocities could act as a catalyst to maintain the thermal comfort for occupants with high metabolic rates to a certain temperature range. Linearity between increased metabolic rates and raised local air velocities is observed in Figure 15a–d. However, change of thermal sensation is seen shifting from left −0.5 range to +0.5 if there is no further increase of local air velocities. Therefore, an acceptable thermal comfort range, i.e., −0.5 to +0.5, can be maintained if we keep increasing air velocities with the increase of temperature. Zhai et al. [41] used multiple fans to systematically study air movement and comfort in warm-humid office environments. The authors included air velocity, temperature, and RH as controlled parameters and concluded that acceptable thermal comfort can be extended to 3 °C by raising air velocities up to 1.8 m/s and 80% RH %. Figure 14 shows that acceptable thermal comfort limit i.e., −0.5 and +0.5 for the occupants, can be extended up to 25 °C with air velocities up to 0.38 m/s. In this study, the ACB unit directs the fixed airflow towards one person (high metabolic rate) at a temperature range of 23–26 °C, whereas the temperatures above 25 °C require even higher airflow directed towards the occupant to maintain thermal comfort range. This may disturb the airflow division in ACB and may cause discomfort for the other occupant in the low velocity zone.

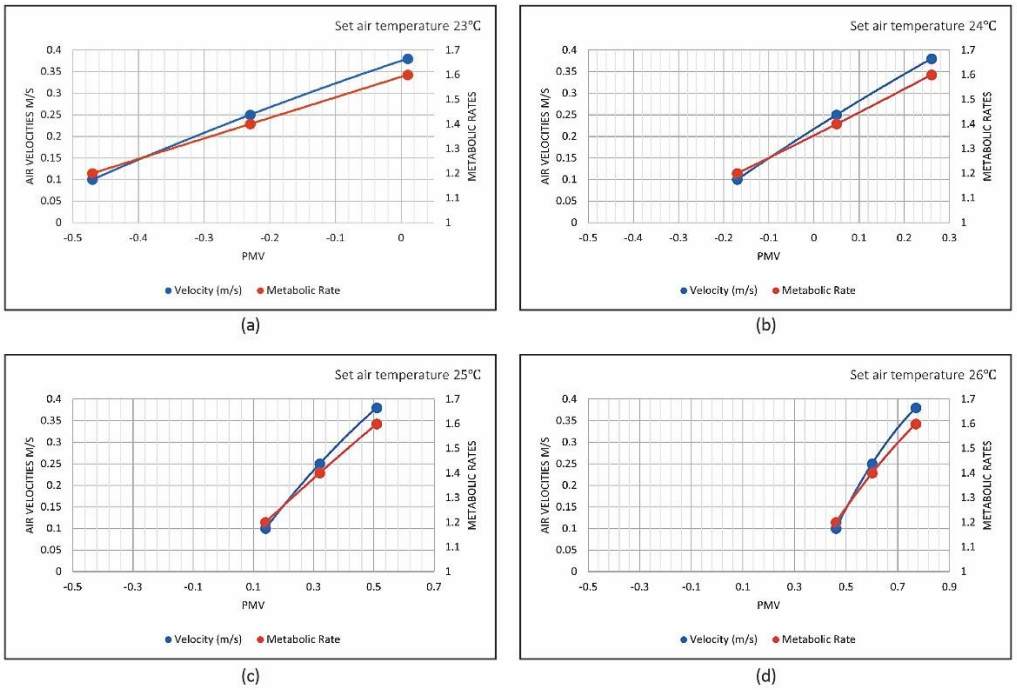

Figure 15. Impact of temperature on thermal comfort for occupants with different metabolic rates. (**a**–**d**): different occupants.

5. Conclusions

This study introduced mixing ventilation in a new way to fulfil individual thermal comfort needs for office occupants with a new precision ventilation system. This precision ventilation system takes the advantages of the mixing ventilation and personalized ventilation to provide individual thermal comfort through efficient air mixing by ACBs. Based on the experimental measurements and CFD simulations of the room with ACB, it can be concluded that ACBs with a JetCone feature can be used for individual thermal comfort applications. High air velocities for the office occupants with elevated metabolic rates and higher room temperatures can maintain acceptable thermal comfort levels. Variations in airflow rates by JetCones lead to significant changes in room air distribution patterns. Two airflow divisions in a room with a single ACB unit led to two different micro-climate velocity zones for two office occupants. The fully opened JetCones produced a longer throw to have higher air velocities up to 0.38 m/s around the occupant, while the decrease in throw through the adjustment pins produced velocities as low as 0.1 m/s around dummies.

The need to compensate different metabolic rates developed the need to establish high and low velocity zones around occupants. Results show that variations in air velocities for a single office zone, for two different occupants (varied metabolic rates), was done with precision by ACB with a JetCone feature. This application of ACB through different JetCones settings provides an innovative way of building micro-climate zones in a single office space through mixing and at the same time eliminates the need of multiple ATDs around the occupant.

6. Limitations and Further Work

This study is done in a small office setup with dual table-chair configuration. In further work, precision ventilation in larger scale offices with multiple ACBs where colliding jets may affect the room air distribution patterns will be studied. The colliding of jets can be used by directing the air to occupants in large scale open-plan offices in order to achieve individual thermal comfort.

Author Contributions: Conceptualization, H.L.; methodology, H.L.; software, P.V.N.; validation, H.L., G.H. and A.A.; formal analysis, H.L.; investigation, H.L.; resources, A.A.; data curation, H.L.; writing—original draft preparation, H.L.; writing—review and editing, S.R. and A.M.; visualization, A.A. and G.H.; supervision, A.A., G.H., S.R. and A.M.; project administration, A.A.; funding acquisition, A.A. All authors have read and agreed to the published version of the manuscript.

Funding: This research received no external funding.

Institutional Review Board Statement: Not applicable.

Informed Consent Statement: Informed consent was obtained from all subjects involved in the study.

Data Availability Statement: The data presented in this study are available on request from the corresponding author.

Acknowledgments: Authors would express their appreciation to Lindab A/S for research support and funding.

Conflicts of Interest: The authors declare no conflict of interest.

Appendix A

Mesh independence test was carried out at line y1 = −0.8·y2 = −1.2 in the middle of the room with different mesh densities. The variations after 1.7 million elements were not found significant and this mesh number was considered suitable for the calculation to avoid computational cost (see Figure A1).

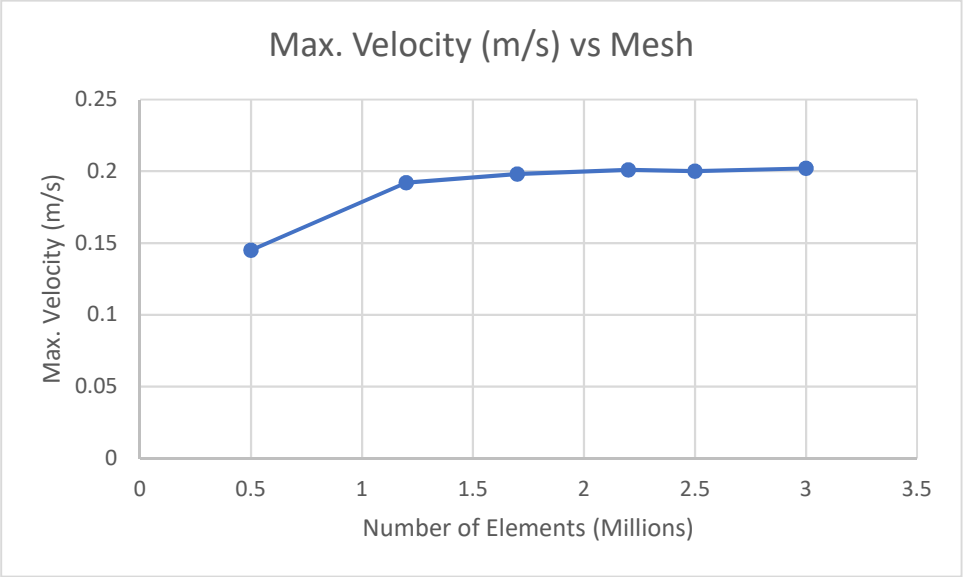

Figure A1. Mesh Independence Test.

The mesh metrics on the horizontal axis in Figure A2 show element quality, where 1 is a perfectly shaped tetrahedral element. Figure A2 shows that most of the elements had a metric range between 0.75 and 0.9. This means that the element quality of the obtained mesh structure is acceptable for carrying out stable numerical computation.

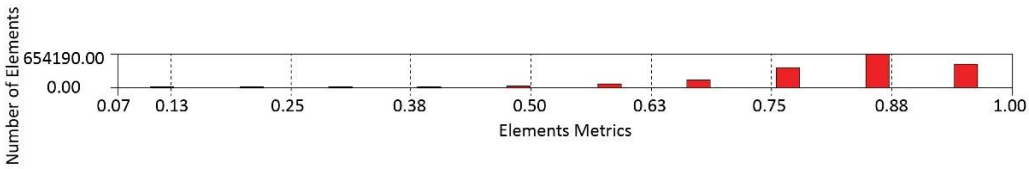

Figure A2. Mesh Element Quality.

The boundary condition in Table A1 were selected with respect to the actual experimental setup used for the measurements. The simulations used the second-order upwind scheme for all the variables (Table A2).

Table A1. Boundary conditions for the simulated model.

Zone	Boundary Type
Inlets	Velocity-inlet
Outlets	Pressure-outlet
Dummy 1	Wall
Dummy 2	Wall
Tables	Wall
Equipment	Wall
Walls	Wall

Table A2. Solution Methods for the simulated model.

Variable	Solution Methods
Scheme	SIMPLE
Gradient	Least Squares Cell Based
Pressure	Second Order
Momentum	Second Order Upwind
Turbulent Kinetic Energy	Second Order Upwind
Turbulent Dissipation Rate	Second Order Upwind
Energy	Second Order Upwind

The air velocities at 12 different points were measured along the length of the room, as shown in Figure 7. These measuring points were taken 1.1 m above the floor. The air velocities at the same fixed positions (as in Figure 7) were measured using probe in CFD post-processing. This experimental and simulation evaluation at these air velocity points was made for case 1 (uniform airflow distribution from ACBs). The measured air velocity points showed a 10% variation from the CFD results as shown in Figure A3.

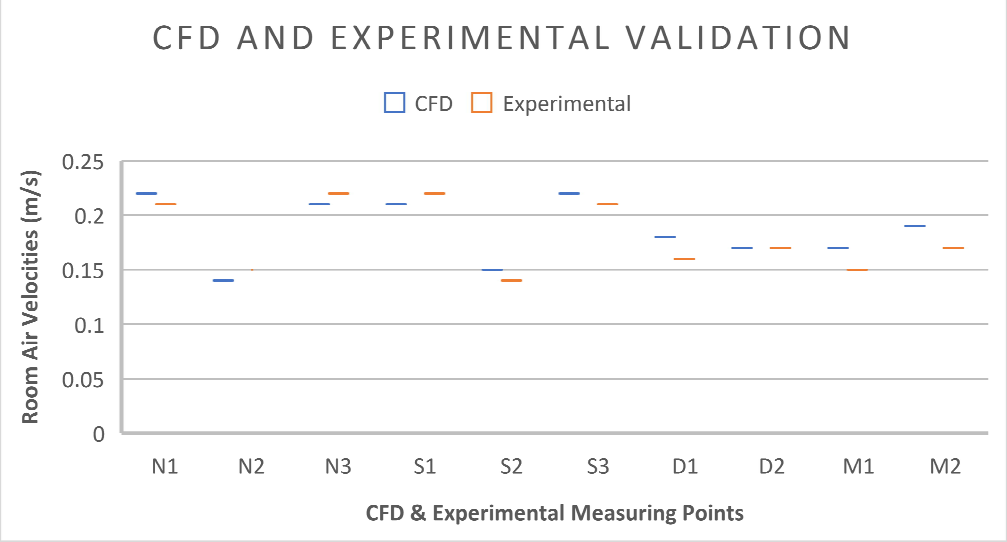

Figure A3. CFD and Experimental validation.

References

1. Gonzalez-Martin, J.; Kraakman, N.J.R. A state–of–the-art review on indoor air pollution and strategies for indoor air pollution control. *Chemosphere* **2021**, *262*, 128376. [CrossRef] [PubMed]
2. Messenger, J.C.; Lee, S.; McCann, D. Trends in working hours, laws, and policies in a global comparative perspective. In *Working Time Around the World*, 1st ed.; Routledge: London, UK, 2007; pp. 22–62.
3. Cao, G.; Awbi, H. A review of the performance of different ventilation and airflow distribution systems in buildings. *Build. Environ.* **2014**, *73*, 171–186. [CrossRef]
4. Wu, B.; Cai, W. Experimental investigation on airflow pattern for active chilled beam system. *Energy Build.* **2018**, *166*, 438–449. [CrossRef]
5. Tritton, D.J. *Physical Fluid Dynamics*, 1st ed.; Springer Science & Business Media: Berkshire, UK, 1977; pp. 30–59.
6. Rhee, K.N.; Shin, M.S. Thermal uniformity in an open plan room with an active chilled beam system and conventional air distribution systems. *Energy Build.* **2015**, *93*, 236–248. [CrossRef]
7. Nicol, J.F.; Roaf, S. Rethinking thermal comfort. *Build. Res. Inf.* **2017**, *45*, 711–716. [CrossRef]
8. Brager, G.; Zhang, H. Evolving opportunities for providing thermal comfort. *Build. Res. Inf.* **2015**, *43*, 274–287. [CrossRef]
9. Wang, Z.; de Dear, R. Individual difference in thermal comfort: A literature review. *Build. Environ.* **2018**, *138*, 181–193. [CrossRef]
10. Djongyang, N.; Tchinda, R. Thermal comfort: A review paper. *Renew. Sustain. Energy Rev.* **2010**, *14*, 2626–2640. [CrossRef]
11. Luo, W.; Kramer, R. The effects of a novel personal comfort system on thermal comfort, physiology and perceived indoor environmental quality, and its health implications-Stimulating human thermoregulation without compromising thermal comfort. *Indoor Air* **2022**, *32*, e12951. [CrossRef]
12. Bluyssen, P.M.; Aries, M. Comfort of workers in office buildings: The European HOPE project. *Build. Environ.* **2011**, *46*, 280–288. [CrossRef]
13. Bluyssen, P.M. Towards new methods and ways to create healthy and comfortable buildings. *Build. Environ.* **2010**, *45*, 808–818. [CrossRef]
14. Karmellos, M.; Kiprakis, A. A multi-objective approach for optimal prioritization of energy efficiency measures in buildings: Model, software and case studies. *Appl. Energy* **2015**, *139*, 131–150. [CrossRef]
15. Veselý, M.; Zeiler, W. Personalized conditioning and its impact on thermal comfort and energy performance–A review. *Renew. Sustain. Energy Rev.* **2014**, *34*, 401–408. [CrossRef]
16. Melikov, A.K.; Cermak, R. Personalized ventilation: Evaluation of different air terminal devices. *Energy Build.* **2002**, *34*, 829–836. [CrossRef]
17. Zhao, W.; Kilpeläinen, S. Thermal environment and ventilation efficiency in a simulated office room with personalized micro-environment and fully mixed ventilation systems. *Build. Environ.* **2021**, *188*, 107445. [CrossRef]
18. Liu, J.; Dalgo, D.A. Performance analysis of a ductless personalized ventilation combined with radiant floor cooling system and displacement ventilation. *Build. Simul.* **2019**, *12*, 905–919. [CrossRef]
19. Ghaddar, N.; Ghali, K. Evaporative cooler improves transient thermal comfort in chilled ceiling displacement ventilation conditioned space. *Energy Build.* **2013**, *61*, 51–60. [CrossRef]
20. Wu, B.; Cai, W. Heat source effects on thermal comfort for active chilled beam systems. *Build. Environ.* **2018**, *141*, 91–102. [CrossRef]
21. Hultmark, G. Supply Air Terminal Device L. U.S. Patent 8876581, 4 November 2014.
22. Zhang, S.; Cheng, Y. Optimization of room air temperature in stratum-ventilated rooms for both thermal comfort and energy saving. *Appl. Energy* **2017**, *204*, 420–431. [CrossRef]
23. *EN 15116:2008*; Rating Standard for the Certification. Eurovent Certification Company: Brussels, Belgium, 2003.
24. Lindab Architect Plexus. *Lindab Plexus Active Chilled Beam, L.*; Lindab A/S: Malmo, Sweden, 2021; p. 15.
25. Latif, H.; Hultmark, G. Performance evaluation of active chilled beam systems for office buildings—A literature review. *Sustain. Energy Technol. Assess* **2022**, *52*, 101999. [CrossRef]
26. Fabbri, K. The indices of feeling—predicted mean vote PMV and percentage people dissatisfied PPD. In *Indoor Thermal Comfort Perception*; Springer: Cesena, Italy, 2015; pp. 75–125.
27. Dawe, M.; Raftery, P. Comparison of mean radiant and air temperatures in mechanically-conditioned commercial buildings from over 200,000 field and laboratory measurements. *Energy Build.* **2020**, *206*, 109582. [CrossRef]
28. Fang, Z.; Lin, Z. Investigation into sensitivities of factors in outdoor thermal comfort indices. *Build. Environ.* **2018**, *128*, 129–142. [CrossRef]
29. Olesen, B.W.; Moreno-Beltrõn, D.L. Target levels. In *Industrial Ventilation Design Guidebook*; Academic Press: Toronto, ON, Canada, 2001; pp. 355–413.
30. Silva, A.S.; Ghisi, E. Performance evaluation of long-term thermal comfort indices in building simulation according to ASHRAE Standard 55. *Build. Environ.* **2016**, *102*, 95–115. [CrossRef]
31. Kristensen, M.H.; Jensen, J.S. Air Temperature Measurements Using Dantec Draught Probes. (DCE Technical Reports No. 189); Department of Civil Engineering, Aalborg University: Aalborg, Denmark, 2015.
32. *Standard EU. EN 13182: 2002*; Ventilation for Buildings—Instrumentation Requirements for Air Velocity Measurements in Ventilated Spaces. European Committee for Standardization: Brussels, Belgium, 2002.

33. Tong, X.; Hong, S.-W. Using CFD simulations to develop an upward airflow displacement ventilation system for manure-belt layer houses to improve the indoor environment. *Biosyst. Eng.* **2019**, *178*, 294–308. [CrossRef]
34. Zhang, Z.; Zhang, W. Evaluation of various turbulence models in predicting airflow and turbulence in enclosed environments by CFD: Part 2—Comparison with experimental data from literature. *HVAC R Res.* **2007**, *13*, 871–886. [CrossRef]
35. Hussain, S.; Oosthuizen, P.H. Evaluation of various turbulence models for the prediction of the airflow and temperature distributions in atria. *Energy Build* **2012**, *48*, 18–28. [CrossRef]
36. Blocken, B. LES over RANS in building simulation for outdoor and indoor applications: A foregone conclusion? *Build. Simul.* **2018**, *11*, 821–870. [CrossRef]
37. Karimi, A. Design Optimization of Active Chilled Beam for an Office Space Using Large Eddy Simulation. In Proceedings of the ASHRAE Winter Conference, Chicago, IL, USA, 1 January 2018.
38. ANSYS Fluent. Available online: www.ansys.com/products/fluids/ansys-fluent (accessed on 22 February 2022).
39. Taghinia, J.H.; Rahman, M.M. Effects of different CFD modeling approaches and simplification of shape on prediction of flow field around manikin. *Energy Build.* **2018**, *170*, 47–60. [CrossRef]
40. Lenzuni, P. Compliance with limits of acceptability for thermal comfort, and implications for long-term comfort. *Build. Environ.* **2021**, *204*, 108067. [CrossRef]
41. Zhai, Y.; Zhang, H. Comfort under personally controlled air movement in warm and humid environments. *Build. Environ.* **2013**, *65*, 109–117. [CrossRef]